Numerical and experimental investigation of temperature effects on the surface plasmon resonance sensor

Kaiqun Lin (林开群)[1,2], Yonghua Lu (鲁拥华)[1,2*], Zhaofeng Luo (罗昭锋)[3], Rongsheng Zheng (郑荣升)[1,2], Pei Wang (王 沛)[1,2], and Hai Ming (明 海)[1,2]**

[1]*Department of Physics, University of Science and Technology of China, Hefei 230026, China*

[2]*Anhui Key Laboratory of Optoelectronic Science and Technology, Hefei 230026, China*

[3]*Test Center of Life Science, University of Science and Technology of China, Hefei 230027, China*

[*]*E-mail: yhlu@ustc.edu.cn;* [**]*e-mail: minghai@ustc.edu.cn*

Received September 12, 2008

The effects of temperature on a surface plasmon resonance (SPR) sensor in Kretschmann configuration are studied experimentally and theoretically. SPR experiments are carried out over a temperature range of 278−313 K in steps of 5 K. A detailed theoretical model is provided to analyze the variation of performance with varying temperature of the sensing environment. The temperature dependence of the properties of the metal, dielectric, and analyte are studied, respectively. The numerical results indicate that the predictions of the theoretical model are well consistent with the experiment data.

OCIS codes: 240.6680, 130.6010, 120.6810.

doi: 10.3788/COL20090705.0428.

Since the first application of the surface plasmon resonance (SPR) phenomenon for sensing technology[1], SPR sensor has been studied intensively because of its high sensitivity and real-time analysis characteristic[2−7]. SPR method has made great progress in terms of both instrumentation development and applications in the past two decades. But in some actual applications like environmental monitoring, there are still challenges such as high cost, bulky size, and the difficulty of temperature regulation at various ambient temperatures.

In reality, the sensor often has to be exposed to environments with varying temperature. Even in the laboratory, fluctuations in ambient temperature can also occur. The temperature of the sensing environment is known to affect SPR sensor significantly through the temperature dependence of the optical properties and thickness of the metal and dielectric[8,9]. And most of the analytes in SPR sensing are aqueous solutions. Since changes in temperature affect the refractive index (RI) of aqueous solutions on the order of 1×10^{-4} RIU/°C (RIU is refractive index unit)[10], a temperature change of 0.1 °C during the detection will cause a change in RI of analyte on the order of 1×10^{-5} RIU. Such small changes can be easily monitored by a SPR sensor which has a RI sensing resolution of 10^{-6}.

In this letter, temperature effects of SPR sensor are studied experimentally and theoretically. We carry out SPR experiments using Biacore3000 optical biosensor (Biacore, Uppsala, Sweden), over a temperature range of 278 − 313 K in steps of 5 K. Then a theoretical model including the temperature dependence of the properties of the metal, dielectric, and analyte layers is applied to simulate our measurements. The experiment data are compared with the numerical results.

The quantitative measurements of the varying response of the SPR sensor at different temperatures are performed using Biacore3000, which is working under angular-interrogation mode. The experimental setup is shown in Fig. 1. Light from a light-emitting diode (λ = 760 nm) is introduced through a TM polarizer, then focused through a prism onto the sensor chip surface in a wedge-shaped beam, giving a fixed range of incident angles. The sensor chip consists of a BK7 optical glass, coated with a gold film (thickness d = 50 nm). Light reflected from the sensor chip is monitored by a linear array of light-sensitive diodes covering the range of incident angles to a resolution of approximately 10^{-5}. The whole optical system is placed in a thermally insulated box, and Peltier elements are used to maintain a constant preset temperature of the system[11].

We carried out SPR experiments over a temperature range of 278 − 313 K in steps of 5 K. For simplicity, a sensor chip with bare gold surface was used in our experiment, and pure water was used as analyte. Figure 2 gives the experimental SPR reflectance curves at different temperatures. In Fig. 2, different pixels correspond to different incident light angles.

Numerical simulation was performed using a comprehensive theoretical model. This model considers the thermal-expansion effect, the phonon-electron scattering, and the electron-electron scattering in the metal along with the thermo-optic effects of the dielectric and

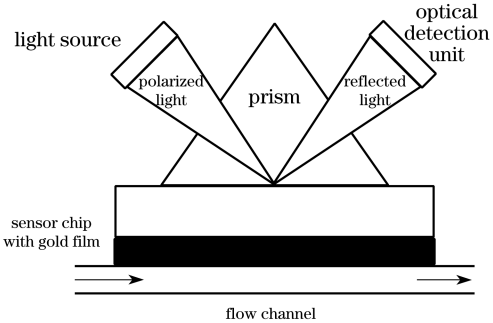

Fig. 1. Experimental setup of SPR sensor system.

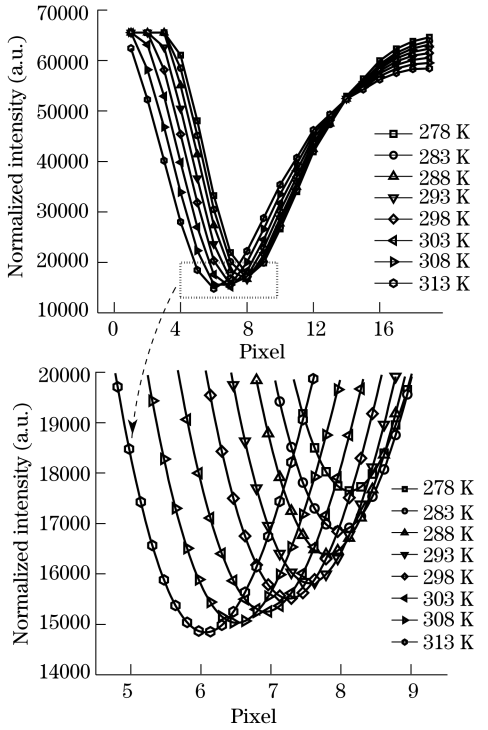

Fig. 2. Experimental SPR curves between normalized intensity and detective pixels at different temperatures.

analyte layers for the variation of the properties of the metal, dielectric, and analyte layers as the temperature changes[8]. The dielectric function of metal layer is modeled using the modified Drude model:

$$\varepsilon(\omega) = \varepsilon(\infty) - \frac{\omega_{\rm p}^2}{\omega(\omega + {\rm i}\omega_{\rm c})}, \tag{1}$$

where $\varepsilon(\infty)$ is the high frequency dielectric function, $\omega_{\rm c}$ is the collision frequency, and $\omega_{\rm p}$ is the plasma frequency. $\omega_{\rm p}$ at a given temperature owing to the thermal expansion effect can be calculated using

$$\omega_{\rm p}(T) = \omega_{\rm p}(T_0)\exp\{-\frac{1}{2}\int_{T_0}^{T}\alpha_{\rm V}(T){\rm d}T\}, \tag{2}$$

where T_0 is the room temperature (300 K) that acts as the reference temperature, and $\alpha_{\rm V}(T)$ is the volumetric thermal expansion coefficient of the metal which also varies with the temperature. According to Debye approximation, $\alpha_{\rm V}(T)$ is written as[12]

$$\alpha_{\rm V}(T) = \frac{\gamma \cdot C_{\rm V}(T)}{K} = \frac{\gamma \cdot 9Nk_{\rm B}\left(\dfrac{T}{T_{\rm D}}\right)^3 \displaystyle\int_0^{T_D/T} \frac{x^4{\rm e}^x}{({\rm e}^x-1)^2}{\rm d}x}{K}, \tag{3}$$

where γ is the Grüneisen constant, N is the density of the conduction electrons, K is bulk modulus, $C_{\rm V}(T)$ is the specific heat at a constant volume, $T_{\rm D}$ is the Debye temperature, and $k_{\rm B}$ is the Boltzmann constant.

The collision frequency $\omega_{\rm c}$ can then be modeled using the phonon-electron scattering model[13] and the electron-electron scattering model[14]. We can thus obtain

$$\begin{aligned}\omega_{\rm c} &= \omega_{\rm ce} + \omega_{\rm cp} \\ &= \frac{1}{6}\pi^4\frac{\Gamma\Delta}{hE_F}\left[(k_{\rm B}T)^2 + \left(\frac{h\omega}{4\pi^2}\right)^2\right] \\ &\quad +\omega_0\left[\frac{2}{5} + 4\left(\frac{T}{T_{\rm D}}\right)^5\int_0^{T_{\rm D}/T}\frac{x^4}{{\rm e}^x-1}{\rm d}x\right],\end{aligned} \tag{4}$$

where $\omega_{\rm ce}$ is the electron-electron scattering frequency, $\omega_{\rm cp}$ is the phonon-electron scattering frequency, ω is the angular frequency of incident light, and $\Gamma\Delta$, ω_0, and E_F are constants.

The variation of thickness of metal film with temperature is written as

$$d(T) = d_0\exp\left\{\int_{T_0}^{T}\alpha'_{\rm L}(T){\rm d}T\right\}, \tag{5}$$

where d_0 is the thickness of the metal film at room temperature, and the corresponding expression of the corrected thermal-expansion coefficient $\alpha'_{\rm L}(T)$ is[15]

$$\alpha'_{\rm L}(T) = \alpha_{\rm L}(T)\frac{1+\mu}{1-\mu}, \tag{6}$$

where μ is the Poisson number of metal, and $\alpha_{\rm L}(T) = \frac{1}{3}\alpha_{\rm V}(T)$ is the linear thermal expansion coefficient of the bulk material.

Now let us come to the temperature effect for the dielectric layer made of BK7 glass. Using a thermo-optic coefficient ${\rm d}n/{\rm d}T$, the temperature-dependent RI at a fixed wavelength can be expressed as

$$n_p(T) = n_p(T_0) + (T - T_0) \times \frac{{\rm d}n}{{\rm d}T}. \tag{7}$$

The situation is more complicated when the dispersion of glass is taken into consideration[9].

Now consider the temperature effect on the analyte. The RI of pure water, as a function of wavelength λ, temperature T, and density ρ, is represented by

$$\begin{aligned}\frac{n^2-1}{n^2+2}(1/\overline{\rho}) = {} & a_0 + a_1\overline{\rho} + a_2\overline{T} + a_3\overline{\lambda}^2\overline{T} \\ & + a_4/\overline{\lambda}^2 + \frac{a_5}{\overline{\lambda}^2 - \overline{\lambda}_{\rm UV}^2} \\ & + \frac{a_6}{\overline{\lambda}^2 - \overline{\lambda}_{\rm IR}^2} + a_7\overline{\rho}^2,\end{aligned} \tag{8}$$

where $\overline{T} = T/T^*$, $\overline{\rho} = \rho/\rho^*$, $\overline{\lambda} = \lambda/\lambda^*$; T^*, ρ^*, λ^*, $a_0 - a_7$, $\overline{\lambda}_{\rm UV}$, and $\overline{\lambda}_{\rm IR}$ are constants[10].

Thus Eqs. (1)–(8) together with the well-known Fresnel equations provide a complete model for the simulation of our measurements. Figure 3 gives the theoretical SPR curves at different temperatures. Both in experimental (Fig. 2) and theoretical curves, two features are noted. Firstly, the resonance angle shifts to smaller values when the temperature increases from 278 to 313 K. A smaller resonance angle means smaller reading of SPR sensor. As shown in Fig. 4, when the temperature increases from 278 to 313 K, the response of the sensor decreases by 3334 RU (3334×10^{-6} RIU) in experimental measurement, and

decreases 3209 RU in numerical simulation. The numerical result is well consistent with the experimental result. Secondly, the SPR curve broadens with the increase of temperature. Broadening of the SPR curve is an important feature because it is directly related to the accuracy of SPR sensor. Figure 5 gives the temperature dependence of the full-widths at half-maximum (FWHMs) of both theoretical and experimental SPR curves. The simulation result is in qualitative agreement with the trends of the experimental data. The curve broadening may be understood in terms of absorption of light power by the gold layer. The imaginary part of the gold dielectric function, which corresponds to the optical absorption, increases with rising temperature in our simulation. This implies the increasing absorption of light power by the gold layer and the broadening of the SPR curve with rising temperature.

To clarify the reason of resonance angle shift, we performed the simulation to separate the temperature effect from the sensor itself and the analyte. Figure 6 shows the serial SPR curves considering only the temperature effect from the sensor itself. It is noted that the resonance angle is a little larger at higher temperature. Comparing these results with the curves in Fig. 3, we find that the temperature effects of the sensor itself and the analyte (water) provide an opposite shift to the resonant position of the SPR curve, and the temperature effect from the analyte is much larger.

In summary, both numerical and experimental approaches are used to investigate the temperature effects on the SPR sensor in Kretschmann configuration. The simulation results indicate that the predictions of theoretical model are well consistent with the experimental data. The SPR curve is shifted and broadened at high temperature because of the change in properties of

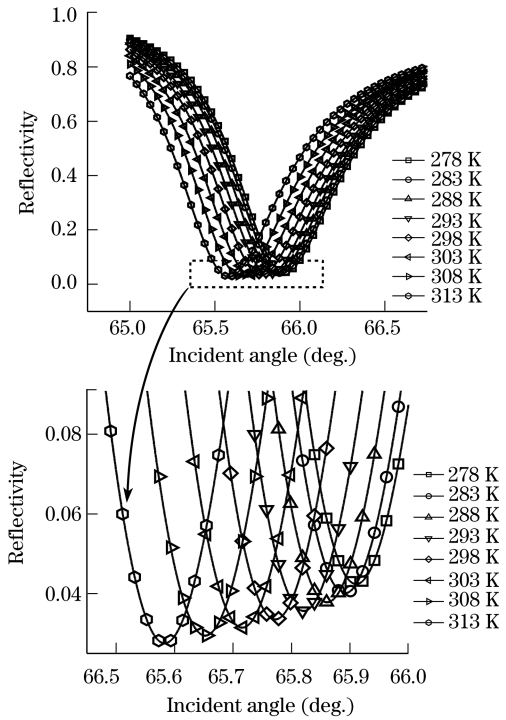

Fig. 3. Theoretical SPR curves between reflectivity and incident angle at different temperatures.

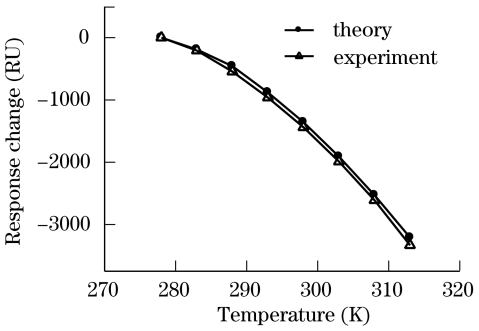

Fig. 4. Change of response of SPR sensor varies with temperature.

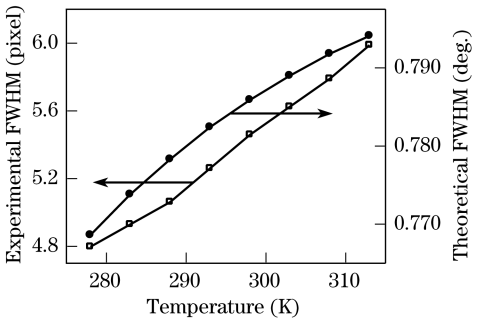

Fig. 5. Variation of FWHM of the SPR curves with temperature.

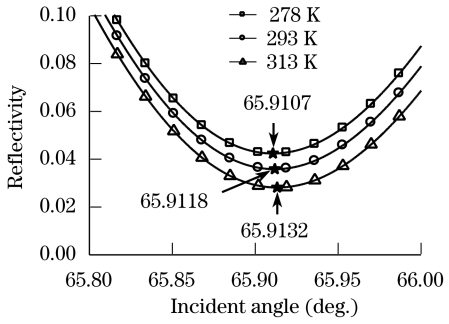

Fig. 6. Numerical SPR curves at 278, 293, and 313 K without considering the change of RI of analyte.

dielectric, metal, and analyte layers, which can be understood from the thermo-optic effect in dielectric and analyte, together with the decrease of plasmon frequency and increase of collision frequency in the metal layer when the temperature increases. When aqueous solutions are used as analyte, the thermal effect of the analyte is much larger than the SPR sensor itself. But in the case of gas detection, the thermal effect from the SPR sensor itself will be comparable to the thermal effect of the analyte. This research may lead to better design and fabrication of SPR sensor against the temperature variation.

This work was supported by the National "973" Program of China (No. 2006CB302905), the Key Program

of National Natural Science Foundation of China (No. 60736037), the National Natural Science Foundation of China (No. 10704070), the National "863" Program of China (No. 2007AA06Z420), and the Science and Technological Fund of Anhui Province for Outstanding Youth (No. 08040106805).

References

1. J. Homola, S. S. Yee, and G. Gauglitz, Sensors and Actuators B **54,** 3 (1999).
2. H. Y. Lin, W. H. Tsai, Y.-C. Tsao, and B. C. Sheu, Appl. Opt. **46,** 800 (2007).
3. Y.-C. Kim, W. Peng, S. Banerji, and K. S. Booksh, Opt. Lett. **30,** 2218 (2005).
4. K. Mitsui, Y. Handa, and K. Kajikawa, Appl. Phys. Lett. **85,** 4231 (2004).
5. L. J. Sherry, R. Jin, C. A. Mirkin, G. C. Schatz, and R. P. Van Duyne, Nano Lett. **6,** 2060 (2006).
6. S.-Y. Wu and H.-P. Ho, Chin. Opt. Lett. **6,** 176 (2008).
7. X. Yang and D. Liu, Chin. Opt. Lett. **5,** 563 (2007).
8. H.-P. Chiang, Y.-C. Wang, P. T. Leung, and W. S. Tse, Opt. Commun. **188,** 283 (2001).
9. K.-Q. Lin, L.-M. Wei, D.-G. Zhang, R.-S. Zheng, P. Wang, Y.-H. Lu, and H. Ming, Chin. Phys. Lett. **24,** 3081 (2007).
10. The International Association for the Properties of Water and Steam, "Release on the refractive index of ordinary water substance as a function of wavelength, temperature and pressure" (IAPWS, Erlangen, 1997) p.2.
11. "Biacore® 3000 instrument handbook" http://www.biacore.com / lifesciences / products / systems_overview/3000/system_information/index.html (Sep. 10, 2008).
12. K. Huang and R. Han, *Solid State Physics* (Higher Education Press, Beijing, 1985).
13. W. E. Lawrence, Phys. Rev. B **13,** 5316 (1976).
14. T. Holstein, Phys. Rev. **96,** 535 (1954).
15. S. Herminghaus and P. Leiderer, Appl. Phys. A **51,** 350 (1990).